# A simple quantum dot: numerical and variational solutions

Connor Walsh, <sup>1,\*</sup> Ian MacPherson, <sup>1</sup> Davidson Joseph, <sup>1</sup> Suyash Kabra, <sup>1</sup> Ripanjeet Singh Toor, <sup>1</sup> Mason Protter, <sup>1</sup> and Frank Marsiglio <sup>1,2,†</sup>

<sup>1</sup>Department of Physics, University of Alberta, Edmonton, AB, Canada T6G 2E1

<sup>2</sup>Theoretical Physics Institute & Quantum Horizons Alberta,
University of Alberta, Edmonton, Alberta T6G 2E1, Canada

We describe a simple quantum dot that consists of two crossed troughs. As such there is no potential well; nonetheless this geometry gives rise to a bound state, centred around the point at which these troughs cross one another. In this paper we review existing numerical methods to solve this problem, and highlight one which we feel is particularly elegant and, in this case, provides the most accurate solution to the problem. The bound state is well-contained on the scale of the trough width, and yields a bound state energy of 0.659606 in units of the minimum continuum state energy. This method also motivates a simple variational solution which yields the lowest energy known to date (0.6812 in the same units) to arise out of an analytical variational solution.

# I. INTRODUCTION

Teaching Quantum Mechanics at an undergraduate level can present several sometimes conflicting goals. One goal is most certainly to instill a desire in the students to pursue the subject further and learn more. Another is to establish some of the elementary results, concepts and methodologies. For example, the solution to the one-dimensional harmonic oscillator is one of the essential problems every student of quantum mechanics should know and understand. Conceptual examples include aspects of wave-particle duality, the notion of a Hilbert space, and the superposition principle embodied in the Schrödinger Cat thought experiment, or more practically in the double-well potential problem. A third goal is to establish a tool kit so that students are prepared to pursue higher-level quantum-mechanical problems. A considerable amount of time can be devoted to this latter goal, and indeed it is typical to devote an entire course to topics such as perturbation theory, WKB Theory, scattering, and many-particle aspects of quantum problems.

These goals can conflict with one another because more interesting problems are often intractable analytically, and approximation schemes to circumvent these difficulties can involve a significant amount of higher-level mathematics. A complementary approach is to utilize numerical solutions to the problem. While numerical solutions have required considerable start-up in the past for the tool kit involved, it is becoming common nowadays for students to already be equipped with computational skills before learning quantum mechanics. Moreover, it is also the case that computational skills are more likely to serve the student in the future compared to an increased knowledge of specialized mathematical functions, regardless of the future career path of the student. At the same time, students can now access more interesting problems that can serve to reinforce the beauty and

novelty of quantum mechanics.

In this paper we will focus on an example of such a problem, involving the existence of a bound state in crossed troughs. This bound state is solely the result of geometric constraints; classically, a bound state does not exist. The potential for this problem is illustrated in Fig. 1.

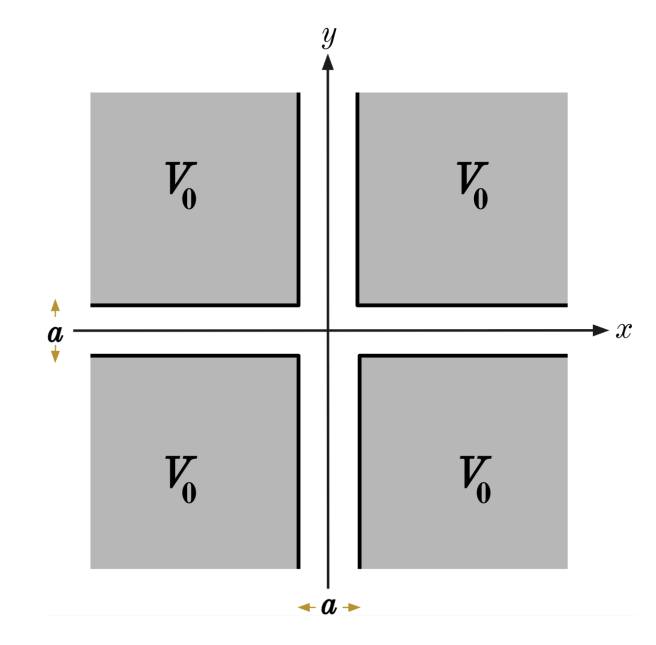


FIG. 1: Schematic of the crossed troughs of width a (shaded in white), with grey-shaded regions with a very large or infinite potential  $(V_0)$  that serves to confine the particle to the troughs. No bound state is expected to exist, classically.

The potential is zero in the white regions along two (one horizontal and one vertical) perpendicular troughs, including the region in which they intersect. These troughs are indicated to extend to  $\pm \infty$  in all four directions, but some of the methods we will discuss to solve this problem require an enclosing box (i.e. a two-dimensional infinite square well) of side length L, where

<sup>\*</sup> cmwalsh@ualberta.ca

 $<sup>^{\</sup>dagger}$  fm3@ualberta.ca

 $L \gg a$ , so that the presence of this confining box does not affect the result for the bound state. In the shaded regions, the value of the barrier potential is given by  $V_0$ , which is assumed to be either very large or infinite. Somewhat surprisingly, this geometry sustains a bound state in the central region, as was illustrated through the variational principle in a problem in Griffiths' Introduction to Quantum Mechanics [1].

We wish to adopt this example as a case study of a problem that is interesting (classically, there is no bound state) and yet is amenable to straightforward numerical solution in a variety of ways. A direct solution to the Schrödinger Equation (SE) is not presented in Griffiths, and that is what we wish to do in the present paper, in a form suitable for undergraduates with access to a diagonalization subroutine, as is available on any computing platform. The primary quantity calculated is the lowest energy eigenvalue, with additional discussion of the lowest energy eigenstate. Even without knowing the form of the wave function, we can surmise that the state is bounded if its energy is lower than the characteristic energy,

$$E_{\rm t} = \frac{\hbar^2 \pi^2}{2m_0 a^2},\tag{1}$$

which gives the minimum threshold (hence the subscript 't') energy for a particle of mass  $m_0$  confined to a one-dimensional infinite well of width a. That is, a particle freely propagating along one of the arms of the cross is necessarily bound in the transverse direction, and thus has an energy at least equal to that of a particle in a one-dimensional square well with barrier height  $V_0$ . As  $V_0 \to \infty$ , this minimum is given by  $E_{\rm t}$ .

We will discuss three distinct numerical methods, (i) matrix mechanics, (ii) finite differences, and (iii) mode-matching. Each of these methods has their distinct advantages, as we will point out below. We will also introduce a simplified model, known as the tight-binding model, and a simple analytical solution, closely related to the mode-matching numerical method.

The outline of this paper is as follows. In Section II we present the solution using matrix mechanics. We consider this the most straightforward and most flexible method. although the usage of matrix mechanics for elementary problems has not yet appeared in undergraduate textbooks. A clear description of the method is provided in Ref. [2], and a two-dimensional generalization can be found in Ref. [3]. The flexibility of this method is apparent in that rounded potentials (i.e. not just potentials with vertical walls) and rounded geometries (not necessarily square geometries as is the case here) can be used with this method. On the other hand, we will require a non-infinite potential and a confining box, as will be described below, but the first of these is actually a more physical feature for the problem, and the second poses no major difficulties.

In Section III we briefly outline the method of finite differences. This methodology is often used to discretize a differential equation so that a matrix problem ensues. A more sophisticated version of this method, called the Relaxation Method, was first presented by Schult et al. [4] to solve this problem (see details of this method in Ref. [5]). This method was further expounded by Londergan and Murdoch [6] in the context of a related model, and then the crossed trough problem was suggested without a solution. We will present a simplified version of this finite-difference method (relaxation is not needed to solve this problem) applied to our crossed trough problem. It turns out that convergence as a function of mesh size is a little slow; moreover this method does not have the flexibility of the previous method, and so is perhaps less desirable.

In Section IV we present the least known and most accurate method for this problem, the so-called mode-matching method. To our knowledge, this method was first discussed in the context of isospectral cavities in Ref. [7], and then also discussed for related problems in Ref. [6]. This method converges very quickly, and is also easy to implement, once the method is understood. For these reasons we devote a little more attention to this method, both in the main text and in the Appendix.

In Section V we examine the simplified problem of crossed single chains, described by a tight-binding model, to illustrate that the physics of a bound state emerges even for this highly simplified case. One can readily compute the energy levels for this problem, and therefore learn of the existence of a bound state. It turns out that the tight-binding model corresponds to the simplest technical implementation of the finite difference method, and therefore the exact solution of this simplified model is related to a crude approximation of one of the three numerical methods.

Finally, in Section VI we close with a simple analytical variational solution that is motivated from the simplest approximation to the mode-matching method. This very simple wave function outperforms (i.e. has a lower energy than) any other known variational solutions.

We close with a summary in Section VII. Although we strive to keep each section self-contained, we have relegated many of the details to the appendices. In this way, we hope the reader can easily follow the main text. At the same time, for the reader interested in one particular technique, the appendices and references should provide sufficient guidance. In addition to the novelty of a quantum bound state where no classically bound state exists, we hope the reader will be motivated to further learn one of the techniques described here and apply it to a new problem. Moreover, the penultimate section also indicates how inspired analytical results can emerge from consideration of numerical results.

#### II. MATRIX MECHANICS

We wish to solve the time-independent Schrödinger equation,

$$-\frac{\hbar^2}{2m_0}\nabla^2\Psi(x,y) + V(x,y)\Psi(x,y) = E\Psi(x,y), \quad (2)$$

for the potential depicted in Fig. 1; however, to use matrix mechanics, modifications are required, and it is necessary to enclose the potential in an infinite two-dimensional square well, i.e. a box of side length L, as depicted in Fig. 6 in Appendix A. Analytically, the potential is now given by

$$V(x,y) = \begin{cases} 0 & |x| < \frac{a}{2} \text{ or } |y| < \frac{a}{2}, \\ V_0 & \frac{a}{2} < |x| < \frac{L}{2} \text{ and } \frac{a}{2} < |y| < \frac{L}{2}, \\ \infty & \text{otherwise,} \end{cases}$$
(3)

so we need  $L \gg a$  for the box to have no influence on the bound state; we find L=5a suffices. It still remains that  $V_0$  should be large compared to any other energy scale in the problem. In particular, having identified  $E_t$  in Eq. (1) (for other reasons), this means  $V_0/E_t \gg 1$ . Here, the reason for the confinement to a two-dimensional box is that it allows us to construct normalizable basis states [2].

Following Ref. [2], we expand the unknown wave function in terms of the known eigenstates of the infinite two-dimensional square box of side length L,

$$\Psi(x,y) = \sum_{m_x=1}^{\infty} \sum_{m_y=1}^{\infty} c_{m_x,m_y} \phi_{m_x,m_y}(x,y), \qquad (4)$$

where

$$\phi_{m_x,m_y}(x,y) \equiv \sqrt{\frac{2}{L}} \sin \left[ \frac{m_x \pi}{L} \left( x + \frac{L}{2} \right) \right] \sqrt{\frac{2}{L}} \sin \left[ \frac{m_y \pi}{L} \left( y + \frac{L}{2} \right) \right]. \tag{5}$$

We rewrite the Schrödinger Equation (2) with this basis, and then take the inner product with an arbitrary basis state [2] (see Appendix A and also Ref. [3] for the two-dimensional version). This procedure results in a simple dimensionless matrix equation,

$$\sum_{m=1}^{\infty} h_{nm} c_m = \epsilon c_n, \tag{6}$$

where  $m \equiv (m_x, m_y)$  and similarly for n, and  $h_{nm}$  and other details of the derivation and truncation procedures are provided in Section A. Diagonalization of  $h_{nm}$  provides eigenvalues  $\epsilon \equiv E/E_{\rm t}$  and eigenvector solutions for a given choice of L, a, and  $V_0$ .

Figure 2 shows the ground state wave function as calculated through the procedure just described, with a/L=0.15 and  ${\rm v_0}\equiv V_0/E_{\rm t}=500$ . It is evident by visual inspection of this figure that the ground state is bounded near the origin where the two troughs intersect.

The wave function has essentially decayed at the boundaries  $(x, y = \pm L/2)$ ; indeed, we have confirmed that for several larger values of L/a, the wave function remains the same. This shows that the box edges at  $\pm L/2$  indeed play no role in the results, as should be the case.

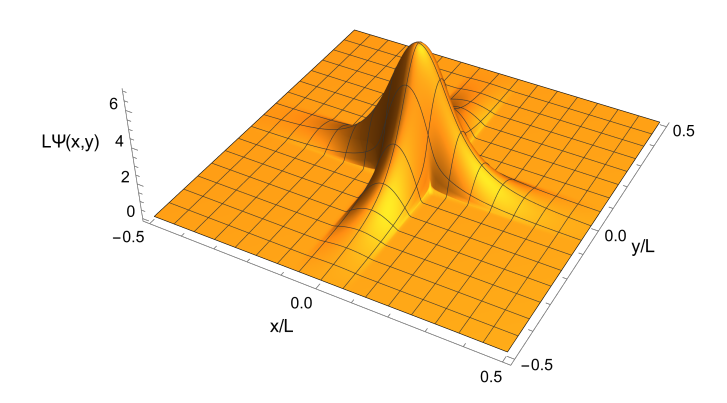


FIG. 2: Ground state wave function, computed with Eq. 4 for a/L=0.15 and  ${\rm v_0}\equiv V_0/E_{\rm t}=500$ . Note that it is self-evidently bounded near the origin. We have confirmed that similar plots are obtained as L/a is increased and for an enormous range of  $V_0$  values.

As an aside at this point, we can ask and answer a question that arises because we have the flexibility to vary  $V_0$  with this method. How universal is the existence of a bound state due to the troughs? In Fig. 3 (main panel, lower set of points) we show the ground state energy, normalized to  $E_t$ , as a function of  $1/\sqrt{v_0}$  (with the actual values of  $v_0$  shown across the top of the graph). Numerical results for a few representative values of  $v_0$  are given by the symbols. Note first that there is very little difference for a/L = 0.1 versus a/L = 0.2. Secondly, the lower set of points are ground state energies E, computed with respect to the infinite  $V_0$  threshold energy,  $E_t$ . As  $V_0$ increases (moving towards the origin in this graph), the energy  $E/E_{\rm t}$  increases. This should happen in general, since the particle is becoming increasingly confined (and therefore *increases* its energy) as  $V_0$  increases. On the other hand, the fact that this state is bounded is caused by the troughs, and the troughs become increasingly welldefined as  $V_0$  increases, suggesting that the state should become more bound (i.e. its energy should decrease) as  $V_0$  increases.

The resolution of this apparent contradiction is that the criterion for boundedness is itself a function of  $V_0$ , as described in Appendix A. For finite  $V_0$ , the relevant threshold energy is the ground state of a finite square well (with strength  $V_0$ ), which we denote by  $E_{\rm t}^{V_0}$ . The upper set of points in Fig. 3 are determined by normalizing the ground state energy to  $E_{\rm t}^{V_0}$ , and these now decrease as  $V_0$  increases, indicating a higher degree of boundedness even though the absolute ground state energy increases

as  $V_0$  increases. This is as we expect. The insert of Fig. 3 shows how the threshold energy  $E_{\rm t}^{V_0}$  varies with  $V_0$ .

We also show a linear fit to these points, as indicated by the lines in both cases. The fact that the points almost form a straight line on this scale is the reason we chose the abscissa to be  $1/\sqrt{\mathbf{v}_0}$  in the first place; while the dependence of  $E_{\rm t}^{V_0}$  on  $\mathbf{v}_0$  (see Eq. (A11)) is suggestive, ultimately this choice was determined empirically.

Our main interest, though, is in the result for  $V_0 \to \infty$ , and the extrapolated result from either fitted straight line in Fig. 3 is clearly close to 0.66, as quoted in Ref. [4]. We can determine this more accurately here, with larger values of  $V_0$ , for example, but we will defer the determination of a more accurate result to the mode-matching method to be described in Sec. IV. Also note that normalizing the bound state energy to the  $V_0$ -dependent threshold energy  $(E_t^{V_0})$  shows that the boundedness is less dependent on  $V_0$  than is implied by the values of  $\epsilon$ .

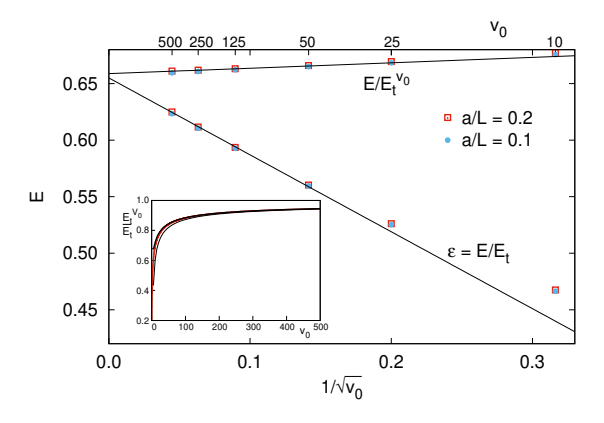


FIG. 3: Bound state energy versus  $1/\sqrt{v_0}$  for a/L=0.2 (unfilled square symbols) and for a/L=0.1 (filled circular symbols). Note that the lower set of symbols shows  $\epsilon \equiv E/E_{\rm t}$ , while the upper set of symbols is a better measure of the boundedness, and plots  $E/E_{\rm t}^{V_0}$ . The actual value of  $v_0 \equiv V_0/E_{\rm t}$  for each symbol is shown across the top of the graph. Note that the variability of  $E/E_{\rm t}^{V_0}$  with  $V_0$  is a lot less than it is for  $\epsilon$ . When the width of the trough is this small there is hardly any dependence on trough width. The inset (red curve) shows the normalized threshold energy,  $E_{\rm t}^{V_0}/E_{\rm t}$  for a bound state as a function of  $v_0$ . The thin black curve gives the first-order analytical expansion (see Eq. (A11) in Appendix A).

In summary, the results shown in this section indicate that matrix mechanics is a relatively straightforward method to obtain bound-state wave functions and energies. This method is more flexible than other methods to be described in the following sections, concerning the characteristics of the potential. For example, here we have explored the possibility of non-infinite barrier potentials and found that boundedness occurs even for relatively shallow potential barriers, and that the degree

of boundedness is surprisingly insensitive to the barrier height.

#### III. FINITE DIFFERENCES

Another standard procedure for obtaining numerically exact solutions to the Schrödinger Equation is to discretize the domain by introducing a grid of points on which to define the wave function, and to approximate all derivatives by their difference formulas. In this section, we shift our focus to the case where  $V_0 \to \infty$ , so the particle becomes perfectly confined to the troughs. In addition, the troughs are terminated at a distance of L/2 from the origin, in all four directions. The Schrödinger Equation now becomes

$$-\frac{\hbar^2}{2m_0}\nabla^2\Psi(x,y) = E\Psi(x,y),\tag{7}$$

defined only on the white regions of Fig. 1, with Dirichlet boundary conditions on the black boundaries and at the trough ends.

Substituting the discrete Laplacian (see Appendix B) into Eq. (7) results in a matrix equation

$$\sum_{i} \bar{L}_{ij} \Psi_j = \epsilon \Psi_i, \tag{8}$$

which relates the unknown values of  $\Psi_i \equiv \Psi(x,y)$  at the interior grid points. Details of the discretization procedure and the matrix  $\bar{L}$  are provided in Section B.

Diagonalization of the sparse matrix  $\bar{L}$  gives numerical approximations to the eigenvalues  $\epsilon \equiv E/E_{\rm t}$  and eigenvector solutions of Eq. (7) for particular choices of L and a; the density of internal grid points is then increased until the numerical results converge to a desired precision. As Table II in Appendix B shows, in the limit  $L/a \to \infty$ , this yields a ground state energy of  $\epsilon = 0.660$ , in agreement with the other methods outlined in this paper.

This method yields good results with minimal effort; however the convergence rate with mesh size is slow, and the flexibility is not as good as the previous method. The calculated energies approach the most accurate ground state energy provided with the mode-matching method, to be described in Section IV. Similarly, the wave functions are very accurate; we do not provide a separate plot as it is indistinguishable from that presented in Sec. II. Small discrepancies with the matrix mechanics result exist because here  $V_0 \to \infty$ , and so no leakage of the wave function outside of the troughs can occur, whereas with finite  $V_0$  some leakage occurs. This will be further explored in Sec. IV.

# IV. MODE-MATCHING METHOD

Another method for tackling such problems is known as mode-matching, and can be used to treat troughs of

either finite or infinite length. Here, we will confine our discussion to troughs of infinite length. For this method it is required that  $V_0 \to \infty$  so that the particle is perfectly confined within the troughs. This time, we do not impose artificial boundaries at  $x=\pm L/2$ , and similarly for y, so that the crossed troughs carry on indefinitely to  $\pm \infty$  in the x- and y-directions, as indicated in Fig. 1. This method also has the benefit of faster numerical convergence than the other two methods presented, and thus has the status of our most accurate solution.

We now seek solutions to Eq. (7), with Dirichlet boundary conditions along the trough walls as well as at  $\pm\infty$ . The geometry is divided into regions, which are shown in Fig. 4 labelled by A through F, on which Eq. (7) can be solved analytically and expressed as a series of Fourier modes. Matching the wave function and its derivatives across the boundaries between regions (denoted by dashed lines) results in a system of equations which relates the expansion coefficients. Solutions to this system of equations give the energies and wave functions that solve Eq. (7).

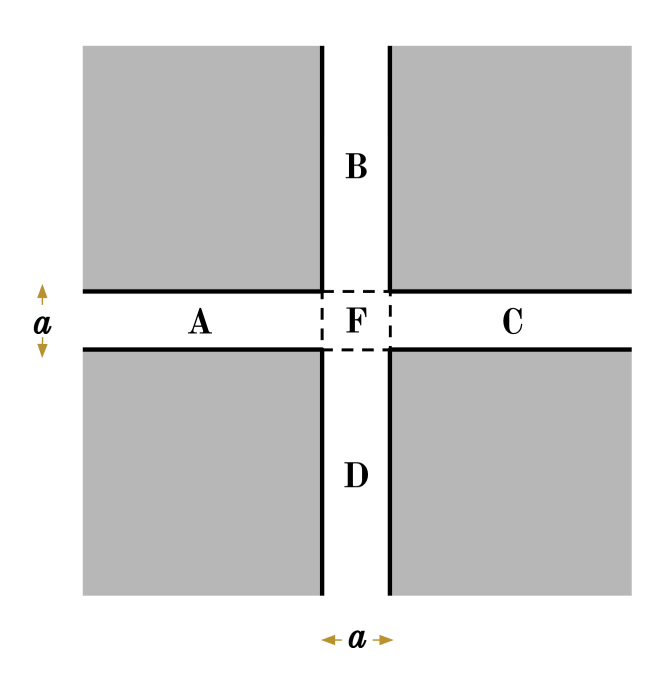


FIG. 4: A sketch of the crossed trough geometry, with labels for the individual regions on which we solve the Schrödinger equation. In our treatment, the arms (regions A, B, C, and D) extend to infinity.

To proceed, we first write down exact solutions that are valid in each of the regions A through F, assuming that  $E < E_t$ ; these solutions are linear combinations of basis states for the different regions, as follows (see Appendix C

for details),

$$\Psi_{\mathcal{A}}(x,y) = \sum_{n=1}^{\infty} A_n e^{\lambda_n \left(\frac{a}{2} + x\right)} \sin\left(\frac{n\pi}{a} \left(y + \frac{a}{2}\right)\right), \tag{9}$$

$$\Psi_{\rm B}(x,y) = \sum_{n=1}^{\infty} B_n e^{\lambda_n \left(\frac{a}{2} - y\right)} \sin\left(\frac{n\pi}{a} \left(x + \frac{a}{2}\right)\right), \quad (10)$$

$$\Psi_{\rm C}(x,y) = \sum_{n=1}^{\infty} C_n e^{\lambda_n \left(\frac{a}{2} - x\right)} \sin\left(\frac{n\pi}{a} \left(y + \frac{a}{2}\right)\right), \quad (11)$$

$$\Psi_{\rm D}(x,y) = \sum_{n=1}^{\infty} D_n e^{\lambda_n \left(\frac{a}{2} - y\right)} \sin\left(\frac{n\pi}{a} \left(x + \frac{a}{2}\right)\right), \quad (12)$$

$$\Psi_{F}(x,y) = \sum_{n=1}^{\infty} A_{n} \frac{\sinh\left(\lambda_{n}\left(\frac{a}{2} - x\right)\right)}{\sinh\lambda_{n}a} \sin\left(\frac{n\pi}{a}\left(y + \frac{a}{2}\right)\right)$$

$$+ \sum_{n=1}^{\infty} B_{n} \frac{\sinh\left(\lambda_{n}\left(\frac{a}{2} + y\right)\right)}{\sinh\lambda_{n}a} \sin\left(\frac{n\pi}{a}\left(x + \frac{a}{2}\right)\right)$$

$$+ \sum_{n=1}^{\infty} C_{n} \sinh\frac{\left(\lambda_{n}\left(\frac{a}{2} + x\right)\right)}{\sinh\lambda_{n}a} \sin\left(\frac{n\pi}{a}\left(y + \frac{a}{2}\right)\right)$$

$$+ \sum_{n=1}^{\infty} D_{n} \frac{\sinh\left(\lambda_{n}\left(\frac{a}{2} - y\right)\right)}{\sinh\lambda_{n}a} \sin\left(\frac{n\pi}{a}\left(x + \frac{a}{2}\right)\right),$$
(12)

where n is a positive integer and  $\lambda_n \equiv \frac{\pi}{a} \sqrt{n^2 - \epsilon}$ , with  $\epsilon \equiv E/E_{\rm t}$ . Notice that by design, this wave function is continuous across the boundaries separating region F from regions A, B, C, and D. Moreover, the four terms for region F were constructed systematically by requiring that each term be non-zero on only one boundary. For example, the first term in Eq. (13) is identically zero at x = a/2 and  $y = \pm a/2$ , but not at x = -a/2. This latter condition is why the coefficient is given by  $A_n$ , the same coefficient as appears in the expression for the wave function for region A (Eq. (9)).

In practice, since the four arms of Fig. 4 are equivalent, the ground state wave function will have even parity, and this symmetry requires that  $A_n = B_n = C_n = D_n$  for all n, simplifying Eqs. (9-13) to

$$\Psi_{A,C}(x,y) = \sum_{n=1}^{\infty} A_n e^{\lambda_n \left(\frac{a}{2} - |x|\right)} \sin\left(\frac{n\pi}{a}\left(y + \frac{a}{2}\right)\right)$$
(14)  

$$\Psi_{B,D}(x,y) = \sum_{n=1}^{\infty} A_n e^{\lambda_n \left(\frac{a}{2} - |y|\right)} \sin\left(\frac{n\pi}{a}\left(x + \frac{a}{2}\right)\right)$$
(15)  

$$\Psi_{F}(x,y) = \sum_{n=1}^{\infty} A_n \frac{\cosh \lambda_n x}{\cosh \frac{\lambda_n a}{2}} \sin\left(\frac{n\pi}{a}\left(y + \frac{a}{2}\right)\right)$$
(16)  

$$+ \sum_{n=1}^{\infty} A_n \frac{\cosh \lambda_n y}{\cosh \frac{\lambda_n a}{2}} \sin\left(\frac{n\pi}{a}\left(x + \frac{a}{2}\right)\right).$$
(16)

In addition, enforcing continuity of the wave function's derivatives (see Appendix C) results in a matrix equation

for the coefficients  $A_n$ :

$$M\mathbf{A} = 0, (17)$$

where

$$M_{mn} \equiv \delta_{mn} \alpha_n \left( 1 + \tanh \alpha_n \right) - \frac{2(2n-1)(2m-1)}{(2n-1)^2 + (2m-1)^2 - \epsilon}$$
(18)

and  $\alpha_n \equiv \frac{\pi}{2} \sqrt{(2n-1)^2 - \epsilon}$ . Here the vector **A** is a column vector containing only the coefficients  $A_n$  corresponding to the even-parity basis states. Details of this calculation are provided in Section C.

Truncating the sums in Eqs. (14) to (16) at a cutoff value N results in a finite matrix in Eq. (17), whose
solutions exist when  $\det M(\epsilon) = 0$ . In practice we guess
a value of  $\epsilon \equiv E/E_{\rm t}$ , diagonalize  $M(\epsilon)$  for that value
of  $\epsilon$ , and then vary  $\epsilon$  until the eigenvalue on the righthand-side of Eq. (17) becomes zero, as required for a
valid solution. As in the matrix mechanics method, the
value of N is increased until the results are converged to
the desired accuracy. In this way, we achieve a ground
state energy of  $\epsilon = 0.659\,606$ . This result is accurate to
the number of digits quoted. When the wave function is
plotted using this method and compared to that shown
in Fig. 2, it is difficult to discern any differences.

To see the differences more clearly, we show in Fig. 5 several one-dimensional slices and compare them to those obtained for  $\mathbf{v}_0 \equiv V_0/E_{\rm t} = 500$  and a/L = 0.15 in Fig. 2. For finite  $V_0$  there are clear differences as a function of x/a for  $y_0 = a/2$ , as an evanescent portion of the wave function exists for |x| > a/2, unlike the  $V_0 \to \infty$  result. The extra weight present in the finite  $V_0$  case has to come from somewhere, and therefore the central maximum is correspondingly lower, as seen most clearly for the  $y_0 = 0$  slice. These differences would be accentuated for even smaller values of  $V_0$ .

One benefit of the mode-matching method is its fast convergence with the truncation value N. Truncating the sums at just a single term (N=1) yields an energy of  $\epsilon=0.681$ , accurate to within approximately 3%, while including just 15 terms yields an error of only  $10^{-3}$ . The N=1 case is of particular interest, as it suggests a natural variational wave function which we explore in Section VI.

In summary, mode-matching is the method best suited to solving the originally posed problem, that is, to find the ground state energy of a particle confined ( $V_0$  is infinite) to two perpendicular troughs extending to  $\pm \infty$  in the x- and y-directions. We find a bound state pictured as in Fig. 2 with energy  $E = 0.659\,606E_{\rm t}$ , where  $E_{\rm t} = \hbar^2 \pi^2/(2m_0 a^2)$ .

# V. TIGHT BINDING

The present problem can also be formulated in a tightbinding formalism, where a particle hops along two intersecting one-dimensional chains of atoms which meet at a single central site with four neighbours. This is best seen as a special case of Fig. 8 in Appendix B where only a single row of internal points is present in the vertical and horizontal directions. It is by no means obvious that two intersecting one-dimensional chains would support a bound state. One problem is that there is no longer a length scale a, corresponding to the transverse trough width, as this has been shrunk to zero.

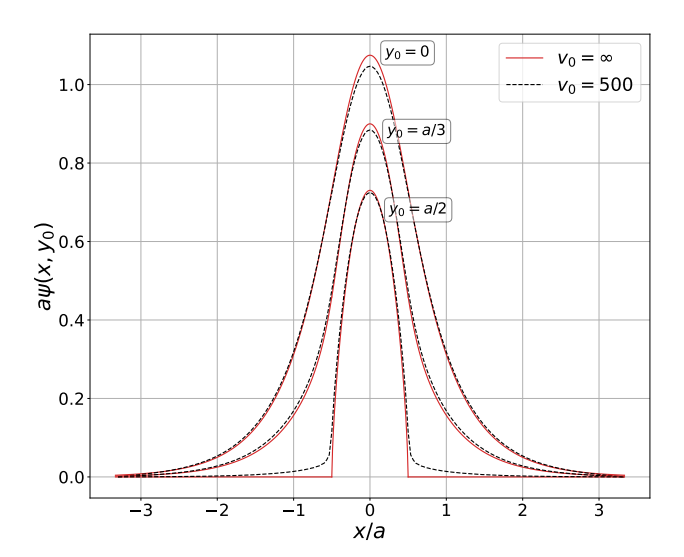


FIG. 5: Ground state wave function for  $L \to \infty$  and  $V_0 \to \infty$  (solid red curves, obtained via mode-matching) and for  $v_0 \equiv V_0/E_t = 500$  and a/L = 0.15 (dashed black curves, obtained via matrix mechanics). Three representative slices of constant y are shown for comparison. For the finite  $V_0$  case, the wave function leaks out of the troughs, which is especially apparent in the  $y_0 = a/2$  curve. This makes the wave function less sharply peaked in the centre, most evident in the  $y_0 = 0$  slice.

We nonetheless proceed. The Hamiltonian is best written in second-quantized form as

$$\hat{H} = -t \sum_{\langle ij \rangle} \left( \hat{c}_i^{\dagger} \hat{c}_j + \hat{c}_j^{\dagger} \hat{c}_i \right), \tag{19}$$

where the sum is carried out over pairs of nearest-neighbour sites, t is the amplitude for hopping between neighbouring sites, and  $\hat{c}_i^{\dagger}$  ( $\hat{c}_i$ ) is the creation (annihilation) operator for a particle at site i.

For a single atomic chain in the thermodynamic limit, the ground state energy is  $E_{\rm t,TB} = -2t$ , where we use the notation  $E_{\rm t,TB}$  in analogy with the threshold energy in the continuum problem (so the subscript t stands for 'threshold', while the additional subscript TB stands for tight-binding). For the crossed-chain geometry, we find through a simple matrix diagonalization a ground state energy of  $E = -2.309t < E_{\rm t,TB}$ , significantly lower than the minimum energy for the single atomic chain, given by  $E_{\rm t,TB} = -2t$ . As was the case with the more complete model, this result indicates that the ground state

is therefore a bound state. These calculations are performed for finite chains of N sites, with periodic boundary conditions, and converged in the thermodynamic limit  $N \to \infty$ . In practice,  $N \gtrsim 30$  is sufficient for convergence.

Interestingly, the tight-binding result turns out to be a low-level of approximation to the finite-difference approximation. As described earlier in Sec. III and in Appendix B, the finite-difference method requires laying down a set of points in the troughs. Table II in Appendix B shows results obtained when N points are used to span the width of a trough, a; tight binding corresponds to the choice of N=1 (not shown in Table II), with  $L\to\infty$  (also not shown). However, the finite-difference method involves a diagonal shift of 4 in the Laplacian (see Eq. (B1) in Appendix B), so the correspondence between  $\epsilon$  as defined for the finite-difference method and E as obtained in the tight-binding model is

$$\epsilon = \frac{4}{\pi^2} \left( \frac{E}{t} + 4 \right). \tag{20}$$

Using our numerical result, E/t = -2.30940 in Eq. (20) gives  $\epsilon = 0.68517$ , which is precisely what we obtain using the finite-difference method with N = 1 and  $L \to \infty$ .

In some sense it is a surprise that the tight-binding approximation yields a bound state, especially since it represents such a crude approximation level for the finite-difference method, but it works qualitatively correctly, and even provides a quantitatively accurate bound state energy.

This result is provided here because it is simple, and because it works both qualitatively and quantitatively. The model used is an effective model, and therefore might not have worked; since it does work, we felt it was worth having this brief discussion.

# VI. VARIATIONAL WAVE FUNCTION

It is clear from the previous sections that we have a very good handle on a complete and accurate solution for the bound ground state in the crossed trough geometry. However, the mode-matching method can be used to generate a very simple variational wave function, by truncating the sum in Eq. (17) at N=1, resulting in

$$\alpha(1 + \tanh \alpha) - \frac{2}{2 - \epsilon} = 0, \tag{21}$$

with  $\alpha = \frac{\pi}{2}\sqrt{1-\epsilon}$ . The solution to this equation is  $\epsilon = 0.6812$ . The wave function (Eqs. (14) to (16)) now becomes very simple to write down:

$$\Psi(x,y) = A \begin{cases} e^{-\lambda|x|} \cos \frac{\pi y}{a}, & (x,y) \in A \text{ or } C \\ e^{-\lambda|y|} \cos \frac{\pi x}{a}, & (x,y) \in B \text{ or } D \end{cases}$$
$$\frac{e^{-\frac{\lambda a}{2}}}{\cosh \frac{\lambda a}{2}} \left[ \cosh \lambda x \cos \frac{\pi y}{a} + \cosh \lambda y \cos \frac{\pi x}{a} \right],$$
$$(x,y) \in F$$
(22)

where we redefined the normalization constant A, and  $\lambda$  has become a variational parameter. Unsurprisingly, minimizing the energy expectation value with respect to  $\lambda$ , (see Section D for details) results in a minimum energy of  $\epsilon=0.6812$ , the same result we achieved from solving Eq. (21). In contrast, the trial wave function given in the textbook problem [1] yields an energy of  $\epsilon=0.7337$ . Our simple wave function, motivated by the mode-matching method, produces a variational wave function that outperforms that given in [1] by a considerable margin. Furthermore, the character of the ground-state wave function achieved by this variational solution is qualitatively accurate, although it does exhibit discontinuities in the derivative of the wave function at the lines connecting the exterior sections of the toughs to the central region.

#### VII. SUMMARY

We have used a number of different methods to study the crossed trough problem. Matrix mechanics, finite-difference methods, and mode-matching constitute a reasonable toolkit for an undergraduate student in physics. Of these, for this particular problem, we have found mode-matching to be the most elegant; it also provides the most accurate solution numerically, and includes the added bonus of providing a natural, simple choice for a variational wave function. The expression for this simple analytical wave function is given in Eq. (22) and has an energy of  $\epsilon = 0.6812$ , quite close to the true ground state energy of  $\epsilon = 0.659606$ .

#### ACKNOWLEDGMENTS

This work was supported in part by the Natural Sciences and Engineering Research Council of Canada (NSERC), and the NSERC Alliance – Alberta Innovates Advance Program.

The authors have no conflicts to disclose.

### Appendix A: Matrix Mechanics Calculation

As was pointed out in Section II, matrix mechanics requires a basis, which is conveniently arranged by embedding the potential represented in Fig. 1 in an infinite two-dimensional square well (i.e. a box) as shown in Fig. 6. The potential representing this confined geometry is given analytically by Eq. (3).

For our actual calculations we shift the coordinates  $x \to x' = x + L/2$  and  $y \to y' = y + L/2$ , so that the wave function given in Eq. (4) uses instead the basis states (we drop the primes)

$$\phi_{m_x,m_y}(x,y) \equiv \sqrt{\frac{2}{L}} \sin\left(\frac{m_x \pi x}{L}\right) \sqrt{\frac{2}{L}} \sin\left(\frac{m_y \pi y}{L}\right),\tag{A1}$$

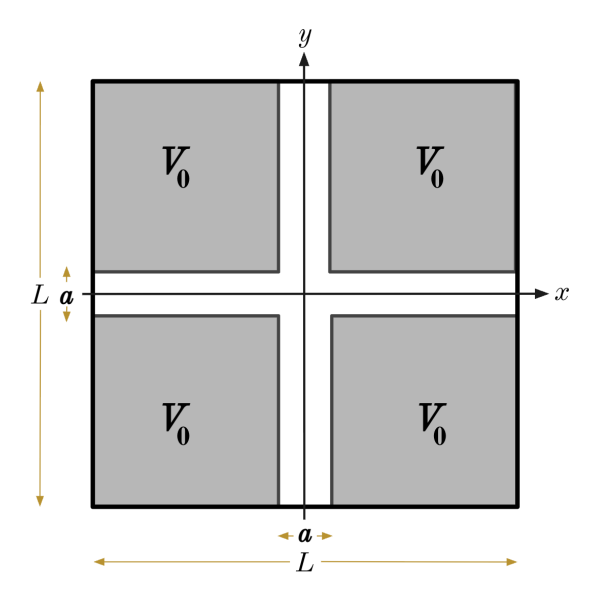


FIG. 6: Schematic of the crossed troughs of width a (shaded in white), with grey-shaded regions with a very large potential  $(V_0)$  that serves to mostly confine the particle to the troughs. The difference from the potential shown in Fig. 1 is that (i) the entire region shown is now embedded in an infinite two-dimensional square well potential indicated by the outer thick black box – the potential is infinite outside of this box, and (ii) a finite (i.e. non-infinite) value for  $V_0$  is required. For a bound state L must be chosen large enough so as not to affect the result in any way. Similarly,  $V_0$  must be chosen large enough to essentially confine the particle to the trough regions.

and now 0 < x, y < L. These shifted functions retain their evenness or oddness, but now with respect to x = L/2 (or y = L/2). We write, in bra-ket notation,

$$H|\psi\rangle = E|\psi\rangle,$$
 (A2)

and then expand  $|\psi\rangle$  in terms of the basis states

$$|\psi\rangle = \sum_{m} c_m |\phi_m\rangle,$$
 (A3)

with  $|\phi_m\rangle$  the ket representation of the basis state given by Eq. (A1) (and remembering that  $m \equiv (m_x, m_y)$  and similarly later for n). If we now construct the inner product of both sides of Eq. (A2) with  $\langle \phi_n|$ , we arrive at the dimensionless matrix equation (having divided both sides by the energy  $E_L \equiv \hbar^2 \pi^2/(2m_0 L^2)$ )

$$\sum_{m=1}^{N} [(h_0)_{nm} + v_{nm}] c_m = e c_n,$$
 (A4)

where  $e \equiv E/E_L$ ,

$$(h_0)_{nm} = \delta_{n_x m_x} \delta_{n_y m_y} (n_x^2 + n_y^2),$$
 (A5)

and the matrix element  $v_{nm}$  is given by  $(v_0 \equiv V_0/E_L)$ 

$$v_{nm} = v_0 \left(\frac{b}{L}\right)^2 I(n_x, m_x) I(n_y, m_y) P(n_x, m_x, n_y, m_y),$$
(A6)

where  $b \equiv (L - a)/2$ . Here,

$$I(n_j, m_j) = \delta_{n_j m_j} \left[ 1 - \operatorname{sinc}\left(\frac{2\pi n_j b}{L}\right) \right] + \left[ 1 - \delta_{n_j m_j} \right] \left[ \operatorname{sinc}\left(\frac{\pi (n_j - m_j) b}{L}\right) - \operatorname{sinc}\left(\frac{\pi (n_j + m_j) b}{L}\right) \right]$$
(A7)

with j = x or y,

$$P(n_x, m_x, n_y, m_y) = 1 + (-1)^{n_y} (-1)^{m_y} + (-1)^{n_x} (-1)^{m_x} + (-1)^{n_y} (-1)^{m_y} (-1)^{n_x} (-1)^{m_x},$$
(A8)

and

$$\operatorname{sinc}(x) \equiv \frac{\sin(x)}{x}.$$
 (A9)

Recall that the two-dimensional box of side length L is artificial, and should not impact the solutions for bound states. Nonetheless,  $E_L$  is the "natural" energy at this stage (it is the energy of the ground state for a onedimensional infinite square well; the ground state for our two-dimensional empty box is therefore  $2E_L$ ). The length L will drop out of all physical results, provided  $L \gg a$ . For numerical calculations, it is clear that the range of the sum in Eq. (A4), in principle infinite, must be truncated at some large cutoff N. This is true for Eq. (4) and (6) as well, so that the matrix becomes of order  $N \times N$ , where  $N = N_{\text{max}} \times N_{\text{max}}$  and  $N_{\text{max}}$  is the cutoff for any one quantum number,  $m_x$  or  $m_y$ . The value of  $N_{\text{max}}$  is increased until the eigenvalues are numerically converged, or we have reached computational limitations. Various symmetries can aid in speed-up. For example, the potential is even about x = L/2 in x and similarly in y, so eigenstates are either even or odd in these variables. If we focus on even eigenstates, which includes the ground state, then only odd integers need be considered in the expansion Eq. (4), and therefore in the matrix equation Eq. (A4). This also implies  $P(n_x, m_x, n_y, m_y) = 4$ . A similar simplification occurs if one considers only eigenstates that have definite  $x \leftrightarrow y$  symmetry.

In Fig. 7 we show the normalized ground state energy  $\epsilon \equiv E/E_{\rm t}$  versus 1/N for a variety of barrier strengths  ${\rm v}_0 \equiv V_0/E_{\rm t}$ , for the case a/L=0.2. Here, the value of N signifies the matrix size without accounting for any symmetries. Symbols indicate the calculated energies for a given matrix size. The results for all potentials look practically horizontal, but in reality there is a dependency on the matrix size N which increases with increasing value of  ${\rm v}_0$ . This is made clearer by expanding the ordinate scale for each value of  ${\rm v}_0$ , and then fitting the results to a linear curve. For example, for the  ${\rm v}_0=125$  results one can plot the same graph on a scale of  $0.59350 < \epsilon < 0.59470$ , and determine (by eye) that  $\epsilon=0.59359+9.0/N$  is a good

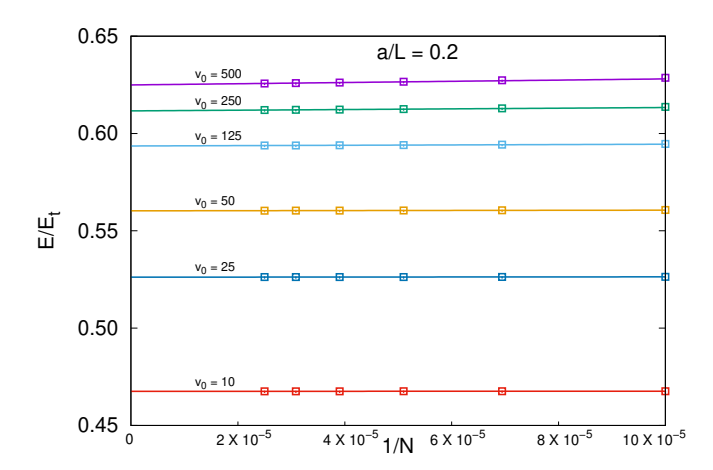


FIG. 7: Normalized energies  $\epsilon \equiv E/E_{\rm t}$  versus 1/N for various values of  ${\rm v_0}$ , for a/L=0.2. Matrices of size  $N\times N$  were used to obtain the results indicated with square symbols. The actual values of N (from right to left on the plot) are 10 000, 14 400, 19 600, 25 600, 32 400, and 40 000. The straight lines were determined by manual fits after expanding the graph for each set of points corresponding to a particular value of  ${\rm v_0}$ . Fit lines are given (in order of increasing value of  ${\rm v_0}$ ) by  $\epsilon=0.4675302+0.51/N$ ,  $\epsilon=0.526185+1.58/N$ ,  $\epsilon=0.560273+3.3/N$ ,  $\epsilon=0.59359+9.0/N$ ,  $\epsilon=0.61162+17.2/N$ , and  $\epsilon=0.62495+31.0/N$ . The  $N\to\infty$  extrapolated values are used in Fig. 3.

fit, particularly to the lowest 3 points, since a reasonable deviation from linearity is now evident on this scale (not shown). The estimated error in intercept value is (conservatively)  $\pm 0.00005$ . There is no need for more rigour since a much more accurate value for the  $V_0 \to \infty$  result is determined by mode-matching. In any event, using the fitted curves to the results in Fig. 7, we find the intercepts as tabulated in the second column of Table I.

$v_0$	$\epsilon$	$E_t^{V_0}/E_t$
10	0.46753	0.6901730
25	0.52619	0.7859253
50	0.56027	0.8412384
125	0.59359	0.8950400
250	0.61162	0.9240440
500	0.62495	0.9453851

TABLE I: The  $N \to \infty$  extrapolated values of  $\epsilon \equiv E/E_{\rm t}$  for  ${\rm v}_0 \equiv V_0/E_{\rm t}$ , for the case a/L=0.2. The estimated error is  $\pm 0.00005$ . These values (2nd column) are shown in Fig. 3 (lower points in the main figure). The third column contains the normalized threshold value  $E_{\rm t}^{V_0}/E_t$ , as determined below and plotted in the insert of Fig. 3. The upper points in Fig. 3 are given by the ratio of the 2nd and 3rd columns in this table.

Table I also contains values of the ground state energy for a single trough with barrier height  $V_0$ . The calculation

for this energy follows that of a single one-dimensional square well (see, e.g. Ref. 1, section 2.6), and requires solution of the transcendental equation

$$\tan(z) = \sqrt{\left(\frac{z_0}{z}\right)^2 - 1},\tag{A10}$$

where  $z\equiv \frac{\pi}{2}\sqrt{E_{\rm t}^{V_0}/E_t}$  and  $z_0\equiv \frac{\pi}{2}\sqrt{{\rm v}_0}$ , with  $E_{\rm t}^{V_0}$  the ground state energy for this problem. A solution for  $E_{\rm t}^{V_0}$  exists no matter how small  $V_0$  is, but this does not automatically imply that a bound state exists in the geometry of the crossed trough (Fig. 1) for arbitrarily small  $V_0$ . The insert in Fig. 3 illustrates how  $E_{\rm t}^{V_0}$  varies with  ${\rm v}_0$  (red curve).

One can expand Eq. (A10) around the  $v_0 \to \infty$  limit, and obtain

$$\frac{E_{\rm t}^{V_0}}{E_t} = 1 - \frac{4}{\pi} \frac{1}{\sqrt{v_0}} + 3\left(\frac{2}{\pi}\right)^2 \frac{1}{v_0} + \dots$$
 (A11)

The thin black curve in the insert of Fig. 3 represents just the first order correction to unity. Including further terms in this expansion makes the result essentially indistinguishable from the numerical solution to Eq. (A10) (thick red curve) on the scale of this insert.

# Appendix B: Finite Difference Calculation

To solve the Schrödinger Equation (7) using finite differences, once more the potential must be truncated at  $x, y = \pm L/2$ . In this case the potential  $V_0$  must be taken to be infinite, so there is no distinction between the shaded grey regions in Fig. 6 and the outer regions. Thus, a faithful depiction of this geometry is shown in Fig. 8. This figure also shows how the domain is discretized by introducing a grid of points, separated by a distance h = a/(N+1), where N is the number of interior grid points spanning the width of each trough. To each of the M interior points (x, y) we associate a variable  $\Psi_{x,y}$  representing the value of the wave function at that point.

We substitute the discrete Laplacian [8]

$$\nabla^2 \Psi(x,y) \approx \frac{\Psi_{x_+,y} + \Psi_{x_-,y} + \Psi_{x,y_+} + \Psi_{x,y_-} - 4\Psi_{x,y}}{h^2},$$
(B1)

where  $x_{\pm} \equiv x \pm h$  and similarly for  $y_{\pm}$ , into Eq. (7) to obtain an equation of the form

$$\left(\frac{N+1}{\pi}\right)^2 \left[4\Psi_{x,y} - \Psi_{x_+,y} - \Psi_{x_-,y} - \Psi_{x,y_+} - \Psi_{x,y_-}\right] = \epsilon \Psi_{x,y}, \tag{B2}$$

with  $\epsilon \equiv E/E_{\rm t}$ , for each of the M variables  $\Psi_{x,y}$ . Together, Eqs. (B2) define rows of the  $M \times M$  matrix Eq. (8), where we set  $\Psi_{x,y} = 0$  for points along the

boundary as necessary, with

$$\bar{L}_{ij} = \left(\frac{N+1}{a}\right)^2 \begin{cases} 4 & \text{if } i=j, \\ -1 & \text{if } i \text{ is next to } j, \\ 0 & \text{otherwise,} \end{cases}$$
(B3)

and  $i, j \equiv (x, y)$ . Equation (8) is then solved by numerical diagonalization, and the resulting eigenvectors are tabulated in Table II.

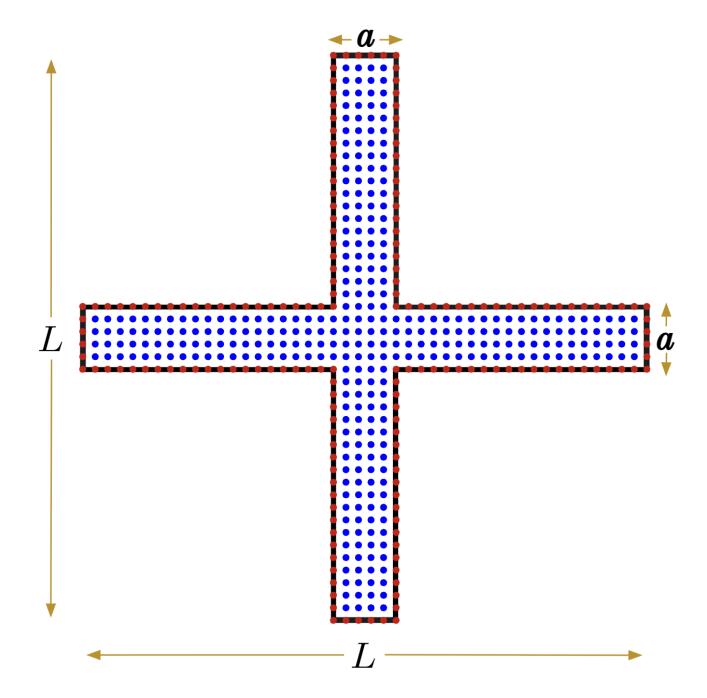


FIG. 8: Grid of points used to discretize the geometry of the problem. Points are separated by a distance h in both the x- and y-directions such that N interior points span the width of each trough (here N=4). Each blue interior point is associated with a variable representing the value of the wave function at that point. Red points on the boundary carry a value of 0 to satisfy the boundary conditions, and are thus only included implicitly.

# Appendix C: Mode-Matching Calculation

Solving the Schrödinger Equation (7) on the regions of Fig. 4 is done by separation of variables, a process familiar to students at the undergraduate level. Assuming a separable solution of the form  $\Psi(x,y) = X(x)Y(y)$ , Eq. (7) becomes

$$Y''(y) = -\phi^2 Y(y),$$
  

$$X''(x) = \lambda^2 X(x),$$
(C1)

for constants  $\phi$  and  $\lambda = \sqrt{\phi^2 - \frac{2mE}{\hbar^2}}$ .

L/a $N$	50	100	200	250	300	350
5	0.66166	0.66063	0.66020	0.66013	0.66008	0.66005
7	$0.66166 \\ 0.66132$	0.66032	0.65990	0.65983	0.65978	0.65975
9	0.66131	0.66031	0.65989	0.65982	0.65978	0.65974
11	0.66131	0.66031	0.65989			

TABLE II: Ground state energy  $\epsilon \equiv E/E_{\rm t}$ , found numerically via finite differences. Rows correspond to a given arm length L in terms of the trough width a. Columns correspond to the number of points used to span each trough. Points on the boundary are not included, so the mesh spacing is h = a/(N+1). As is clear from examining the second and third rows, making the arms three times as long as they are wide (L=7a) is sufficient to converge the results to 4 decimal places. This is essential for the success of this method, as the number of points grows quickly with L. For comparison, our most accurate result is  $\epsilon = 0.659606$ , found with the mode-matching method.

Consider region A for definiteness. For  $\Psi$  to vanish on both edges of the trough, Y(y) must take the form

$$Y_n(y) = \sin\left(\phi_n\left(y + \frac{a}{2}\right)\right), \quad n = 1, 2, \dots,$$
 (C2)

with  $\phi_n = n\pi/a$ . For a bound state to exist, we need  $E < E_t$  which implies  $\lambda^2 > 0$ , and therefore

$$X_n(x) = e^{\lambda_n \left(\frac{a}{2} + x\right)},\tag{C3}$$

where now  $\phi$  and  $\lambda$  have acquired a dependence on the quantum number n, and we have used only the one solution that remains finite as  $x \to -\infty$ . The general solution on region A is the linear combination

$$\Psi_{\mathcal{A}}(x,y) = \sum_{n=1}^{\infty} A_n e^{\lambda_n \left(\frac{a}{2} + x\right)} \sin\left(\frac{n\pi}{a} \left(y + \frac{a}{2}\right)\right), \quad (C4)$$

with arbitrary coefficients  $A_n$ . Solutions in regions B, C, and D are found in a similar manner.

Region F has no external boundaries at which to impose boundary conditions, so we consider four separate boundary-value problems such that

$$\Psi_{\rm F} = \Psi_{\rm F_A} + \Psi_{\rm F_B} + \Psi_{\rm F_C} + \Psi_{\rm F_D},\tag{C5}$$

where  $\Psi_{F_A}$  vanishes on all boundaries of F except its border with region A;  $\Psi_{F_B}$  is nonzero only on the border

with B; and so on. Again, the condition  $\lambda_n^2 > 0$  leads to

$$\Psi_{F}(x,y) = \sum_{n=1}^{\infty} A'_{n} \sinh\left(\lambda_{n}\left(\frac{a}{2} - x\right)\right) \sin\left(\frac{n\pi}{a}\left(y + \frac{a}{2}\right)\right)$$

$$+ \sum_{n=1}^{\infty} B'_{n} \sinh\left(\lambda_{n}\left(\frac{a}{2} + y\right)\right) \sin\left(\frac{n\pi}{a}\left(x + \frac{a}{2}\right)\right)$$

$$+ \sum_{n=1}^{\infty} C'_{n} \sinh\left(\lambda_{n}\left(\frac{a}{2} + x\right)\right) \sin\left(\frac{n\pi}{a}\left(y + \frac{a}{2}\right)\right)$$

$$+ \sum_{n=1}^{\infty} D'_{n} \sinh\left(\lambda_{n}\left(\frac{a}{2} - y\right)\right) \sin\left(\frac{n\pi}{a}\left(x + \frac{a}{2}\right)\right).$$
(C6)

Matching the wave function along the dashed boundary lines gives a simple relation between the primed coefficients in Eq. (C6)and their un-primed counterparts in the corresponding troughs. For example, concerning the term in F that shares a boundary with region A, we have  $A'_n = A_n/\sinh(\lambda_n a)$ , and similarly for the other coefficients.

The wave function's derivative must also be continuous across inter-region boundaries. We take the inner product of this condition with appropriate sine functions to arrive at

$$\int_{-\frac{a}{2}}^{\frac{a}{2}} dy \sin\left(\frac{m\pi}{a}\left(y + \frac{a}{2}\right)\right) \left[\frac{\partial \Psi_{A}}{\partial x} - \frac{\partial \Psi_{F}}{\partial x}\right]_{x = -\frac{a}{2}} = 0,$$

$$\int_{-\frac{a}{2}}^{\frac{a}{2}} dx \sin\left(\frac{m\pi}{a}\left(x + \frac{a}{2}\right)\right) \left[\frac{\partial \Psi_{B}}{\partial y} - \frac{\partial \Psi_{F}}{\partial y}\right]_{y = \frac{a}{2}} = 0,$$

$$\int_{-\frac{a}{2}}^{\frac{a}{2}} dy \sin\left(\frac{m\pi}{a}\left(y + \frac{a}{2}\right)\right) \left[\frac{\partial \Psi_{C}}{\partial x} - \frac{\partial \Psi_{F}}{\partial x}\right]_{x = \frac{a}{2}} = 0,$$

$$\int_{-\frac{a}{2}}^{\frac{a}{2}} dx \sin\left(\frac{m\pi}{a}\left(x + \frac{a}{2}\right)\right) \left[\frac{\partial \Psi_{D}}{\partial y} - \frac{\partial \Psi_{F}}{\partial y}\right]_{y = -\frac{a}{2}} = 0.$$
(C7)

Due to symmetry, the equations in Eq. (C7) are all equivalent; performing the derivatives in the first equation, for example, gives

$$A_m \frac{\lambda_m a}{2} \left( 1 + \tanh \frac{\lambda_m a}{2} \right) - \sum_{n=1}^{\infty} A_n \rho_{mn} = 0$$
 (C8)

for all integers  $m \geq 1$ , where

$$\rho_{mn} \equiv \frac{1 - (-1)^m}{\sinh \lambda_n a} \frac{n\pi}{a} \int_{-\frac{a}{2}}^{\frac{a}{2}} dy \sinh\left(\lambda_n \left(\frac{a}{2} + y\right)\right) \sin\left(\frac{m\pi}{a} \left(y + \frac{a}{2}\right)\right) \\
= \frac{1 - (-1)^m}{2} \frac{2nm}{n^2 + m^2 - \epsilon},$$
(C0)

with  $\epsilon \equiv E/E_{\rm t}$ . Putting this in the form of a matrix equation yields

$$(D - \rho)\mathbf{A} = 0, \tag{C10}$$

with

$$D_{mn} \equiv \delta_{nm} \frac{\lambda_n a}{2} \left( 1 + \tanh \frac{\lambda_n a}{2} \right), \quad (C11)$$

$$\rho_{mn} \equiv \frac{1 - (-1)^m}{2} \frac{2nm}{m^2 + n^2 - \epsilon}.$$
 (C12)

Finally, symmetry requires that  $A_n=0$  for all even n, since these modes have odd symmetry with respect to reflections across the coordinate axes. For this reason, all even rows of the matrix can be removed, and Eq. (C10) can be written more compactly in a symmetric form as Eq. (17).

# Appendix D: Variational Wave Function

The wave function in Eq. (22) can be normalized analytically, though the algebra is somewhat tedious. The arms are symmetric so we need only integrate over one of them (say, region C in Fig. 4):

$$\int_{F} |\Psi_{F}(x,y)|^{2} + 4 \int_{C} |\Psi_{C}(x,y)|^{2} \stackrel{!}{=} 1.$$
 (D1)

The integrals here are all elementary, and therefore from Eq. (D1) we have

$$A^{2} = \frac{e^{\lambda a}}{a^{2}} \left[ \frac{1}{\lambda a} \left( 1 + \tanh \frac{\lambda a}{2} \right) + \frac{1}{2} \operatorname{sech}^{2} \frac{\lambda a}{2} + \frac{8\pi^{2}}{\left(\pi^{2} + a^{2}\lambda^{2}\right)^{2}} \right]^{-1}.$$
(D2)

We next consider the expectation value of the Hamiltonian. Because the variational wave function (unlike the infinite sum in Eq. (13)) is discontinuous across region boundaries, the integral must be explicitly evaluated across these boundaries, as well as on the interior of the regions in Fig. 4. Again using symmetry,

$$\langle \hat{H} \rangle = -\frac{\hbar^2}{2m_0} \left[ \int_{\mathcal{F}} \Psi_{\mathcal{F}}(x, y) \nabla^2 \Psi_{\mathcal{F}}(x, y) + 4 \int_{\mathcal{C}} \Psi_{\mathcal{C}}(x, y) \nabla^2 \Psi_{\mathcal{C}}(x, y) + 4 \lim_{\epsilon \to 0} \int_{\frac{a}{2} - \epsilon}^{\frac{a}{2} + \epsilon} dx \int_{-\frac{a}{2}}^{\frac{a}{2}} dy \, \Psi(x, y) \nabla^2 \Psi(x, y) \right].$$
(D3)

The integrals over individual regions are evaluated easily by exploiting the fact that, by construction, the wave functions are eigenfunctions of the Laplacian, so we have

$$\int_{F} \Psi_{F}(x,y) \nabla^{2} \Psi_{F}(x,y) + 4 \int_{C} \Psi_{C}(x,y) \nabla^{2} \Psi_{C}(x,y) 
= \left[ \lambda^{2} - \frac{\pi^{2}}{a^{2}} \right] \underbrace{\left[ \int_{F} \left| \Psi_{F}(x,y) \right|^{2} + 4 \int_{C} \left| \Psi_{C}(x,y) \right|^{2} \right]}_{=1}.$$
(D4)

For the boundary integral, we write the wave function in the vicinity of the boundary between regions C and F as

$$\Psi(x,y) = A \left[ e^{-\lambda x} \cos \frac{\pi y}{a} \theta \left( x - \frac{a}{2} \right) + \frac{e^{-\frac{\lambda a}{2}}}{\cosh \frac{\lambda a}{2}} \left[ \cosh \lambda x \cos \frac{\pi y}{a} + \cosh \lambda y \cos \frac{\pi x}{a} \right] \theta \left( \frac{a}{2} - x \right) \right]. \tag{D5}$$

Then

$$\frac{\partial \Psi}{\partial x} = A \left\{ -\lambda e^{-\lambda x} \cos \frac{\pi y}{a} \theta \left( x - \frac{a}{2} \right) + \frac{e^{-\frac{\lambda a}{2}}}{\cosh \frac{\lambda a}{2}} \left[ \lambda \sinh \lambda x \cos \frac{\pi y}{a} - \frac{\pi}{a} \cosh \lambda y \sin \frac{\pi x}{a} \right] \theta \left( \frac{a}{2} - x \right) \right. \\
+ \left. \left( \left[ e^{-\lambda x} - \frac{e^{-\frac{\lambda a}{2}}}{\cosh \frac{\lambda a}{2}} \cosh \lambda x \right] \cos \frac{\pi y}{a} - \frac{e^{-\frac{\lambda a}{2}}}{\cosh \frac{\lambda a}{2}} \cosh \lambda y \cos \frac{\pi x}{a} \right) \delta \left( x - \frac{a}{2} \right) \right\}. \tag{D6}$$

The last term (second line proportional to the  $\delta$ -function) can be dropped because the quantity in parentheses vanishes at x = a/2. Indeed, any function f(x) for which  $f(x_0) = 0$  satisfies  $f(x_0)\delta(x - x_0) \equiv 0$  even after taking further derivatives, since for arbitrary g(x) we have

$$\int dx \, g \frac{d}{dx} \Big( f \delta(x - x_0) \Big) = \int dx \, \Big( g f' \delta(x - x_0) + g f \frac{d}{dx} \delta(x - x_0) \Big) 
= g(x_0) f'(x_0) + g(x) f(x) \delta(x - x_0) - \int dx \, (g f)' \delta(x - x_0) = g(x_0) f'(x_0) - g'(x_0) f(x_0) - g(x_0) f'(x_0) = 0.$$
(D7)

Taking another derivative,

$$\begin{split} \frac{\partial^2 \Psi}{\partial^2 x} &= A \Bigg\{ \lambda^2 e^{-\lambda x} \cos \frac{\pi y}{a} \theta \Big( x - \frac{a}{2} \Big) + \frac{e^{-\frac{\lambda a}{2}}}{\cosh \frac{\lambda a}{2}} \Big[ \lambda^2 \cosh \lambda x \cos \frac{\pi y}{a} - \Big( \frac{\pi}{a} \Big)^2 \cosh \lambda y \cos \frac{\pi x}{a} \Big] \theta \Big( \frac{a}{2} - x \Big) \\ &- \bigg( \Big[ \lambda e^{-\lambda x} + \frac{e^{-\frac{\lambda a}{2}}}{\cosh \frac{\lambda a}{2}} \lambda \sinh \lambda x \Big] \cos \frac{\pi y}{a} - \frac{\pi}{a} \frac{e^{-\frac{\lambda a}{2}}}{\cosh \frac{\lambda a}{2}} \cosh \lambda y \sin \frac{\pi x}{a} \Big) \delta \Big( x - \frac{a}{2} \Big) \Bigg\}. \end{split} \tag{D8}$$

Since we take the range of integration around x=a/2 to be  $\epsilon/2\to 0$ , only the  $\delta$ -function terms in Eq. (D8) will survive in the final result. For the same reason, all terms coming from the y-derivative vanish in the limit. The remaining integral is

$$\begin{split} &\int_{\frac{a}{2}-\epsilon}^{\frac{a}{2}+\epsilon} dx \int_{-\frac{a}{2}}^{\frac{a}{2}} dy \, \Psi(x,y) \nabla^2 \Psi(x,y) \\ = &A \int_{\frac{a}{2}-\epsilon}^{\frac{a}{2}+\epsilon} dx \int_{-\frac{a}{2}}^{\frac{a}{2}} dy \, \Psi(x,y) \bigg( - \bigg[ \lambda e^{-\lambda x} + \frac{e^{-\frac{\lambda a}{2}}}{\cosh \frac{\lambda a}{2}} \lambda \sinh \lambda x \bigg] \cos \frac{\pi y}{a} - \frac{\pi}{a} \frac{e^{-\frac{\lambda a}{2}}}{\cosh \frac{\lambda a}{2}} \cosh \lambda y \sin \frac{\pi x}{a} \bigg) \delta \bigg( x - \frac{a}{2} \bigg) \\ = &A \int_{-\frac{a}{2}}^{\frac{a}{2}} dy \, \Psi \bigg( \frac{a}{2}, y \bigg) \bigg( -\lambda e^{-\frac{\lambda a}{2}} \bigg[ 1 + \tanh \frac{\lambda a}{2} \bigg] \cos \frac{\pi y}{a} - \frac{\pi}{a} \frac{e^{-\frac{\lambda a}{2}}}{\cosh \frac{\lambda a}{2}} \cosh \lambda y \bigg) \\ = &A^2 \left[ -\frac{\lambda a}{2} \bigg( 1 + \tanh \frac{\lambda a}{2} \bigg) + \frac{2\pi^2}{\pi^2 + \lambda^2 a^2} \right]. \end{split} \tag{D9}$$

All together, Eq. (D3) becomes

$$\langle \hat{H} \rangle = \frac{\hbar^2 \pi^2}{2ma^2} \left[ 1 - \frac{\lambda^2 a^2}{\pi^2} + \frac{4}{\pi^2} \frac{\frac{\lambda a}{2} \left( 1 + \tanh \frac{\lambda a}{2} \right) - \frac{2\pi^2}{\pi^2 + \lambda^2 a^2}}{\frac{1}{\lambda a} \left( 1 + \tanh \frac{\lambda a}{2} \right) + \frac{1}{2} \operatorname{sech}^2 \frac{\lambda a}{2} + \frac{8\pi^2}{\left(\pi^2 + a^2 \lambda^2\right)^2}} \right]. \tag{D10}$$

The minimum value of this expression is found numerically to be  $\langle \hat{H} \rangle_{\min} = 0.6812 E_{t}$ , achieved when  $\lambda = 1.7738/a$ ; this is precisely the result achieved via Eq. (21). Alternatively, taking the derivative of Eq. (D10) with respect to  $\lambda$ , and setting the result to zero, one finds, after much algebra, the result

$$\lambda a \left( 1 + \tanh \frac{\lambda a}{2} \right) = \frac{4}{1 + \left( \frac{\lambda a}{\pi} \right)^2},\tag{D11}$$

which, taken with Eq. (D10), is precisely Eq. (21) for  $\alpha = \lambda a/2$ .

- [1] D.J. Griffiths, "Introduction To Quantum Mechanics, 3rd Edition", (Cambridge University Press, Cambridge, 2018). See Problem 8.27, titled "Quantum Dots", where a variational solutions is presented, and it is demonstrated that this solution has a lower energy than any of the propagating (i.e. unbound) solutions. Note that the 2nd edition of this same book has another (slightly inferior) solution.
- [2] F. Marsiglio, "The harmonic oscillator in quantum mechanics: A third way", Amer. J. Phys. 77, 253-258 (2009).
- [3] R.L. Pavelich and F. Marsiglio, "Calculation of 2D electronic band structure using matrix mechanics", Amer. J. Phys. 84, 924-935 (2016).
- [4] R. L. Schult, D. G. Ravenhall, and H. W. Wyld, "Quantum bound states in a classically unbound system of crossed wires," Phys. Rev. B39, 5476-5479 (1989).

- [5] William H. Press, Brian P. Flannery, Saul A. Teukolsky, and William T. Vetterling, "Numerical Recipes: The Art of Scientific Computing", (Cambridge University Press, Cambridge, 1986). See Chap. 17.5, page 652.
- [6] J.T. Londergan and D.P. Murdoch, "Confined modes in two-dimensional tubes", Amer. J. Phys. 80, 1085-1093 (2012).
- [7] Hua Wu, D.W.L. Sprung and J. Martorell, "Numerical investigation of isospectral cavities built from triangles", Phys. Rev. bf E51, 703-708 (1995).
- [8] M. Abramowitz and I. A Stegun, "Handbook of Mathematical Functions with Formulas, Graphs, and Mathematical Tables, 9th Edition", (Dover Publications, New York, 1970). See Chap. 25, page 885.